ELSEVIER

Static Green's functions in multilayered half spaces

Ernian Pan

Department of Civil Engineering, University of Colorado, Boulder, CO, USA

This paper presents an efficient and accurate method for the calculation of static Green's functions in a multilayered transversely isotropic or isotropic half space. The cylindrical system of vector functions and the propagator matrix method are used to derive the Green's functions in the transformed domain. The well-known exponentially growing elements in the propagator matrix are fractionated out by propagating the matrix either upwards or downwards, depending upon the relative vertical location of the source and field points. The Green's functions in the physical domain are evaluated numerically by an adaptive Gauss quadrature with continued fraction expansions. Numerical examples are presented to show that very accurate Green's functions with relatively less Gauss quadrature points can be obtained. These examples also show clearly the effect of material layering and anisotropy on the displacement and stress fields. © *1997 by Elsevier Science Inc.*

Keywords: Green's function, multilayered half space, transverse isotropy

1. Introduction

Since many physical problems can be modeled as a layered system a lot of research has been carried out related to layered structures. These studies cover the areas of piezoelectricity,[1] thermomechanics,[2,3] microelectronics,[4,5] electronomagnetics,[6] poroelasticity,[7,8] viscoelasticity,[9,10] elastostatics,[11-13] and finally, elastodynamics.[14-16]

Numerically, layered structures can be analyzed by either the domain-discretization methods (e.g., the FEM) or the boundary element method (BEM). The latter, however, is more suited than the former to cases where better accuracy is required due to problems such as stress concentrations or where the domain of interest extends to infinity. It is noted that when solving problems in a layered system the beauty and main advantage of the BEM (i.e., discretization of the problem on boundaries only) may be lost if one approaches the problem by the sub-domain method (i.e., discretizing along each interface combined with suitable continuity conditions there). An alternative approach that can strictly preserve the BEM's beauty and main advantage is to apply the BEM formulation to the layered system with the Green's functions being those in the layered system instead of being those in a homogeneous and infinite domain. By so doing, no discretization along each interface is necessary while each layer is strictly discrete. Therefore the key point in the BEM modeling of layered systems is to provide the Green's functions for such systems.

Previously, several approaches have been suggested for calculating the required Green's functions in the layered system for the BEM:

The first method is the state-space approach (or the mixed method of elastodynamics) as studied by Bahar,[17] Rao and Das,[18] Abhyankar and Chandrashekara,[19] and Chandrashekara and Santhosh[20] for the elastodynamic case. In this method solutions are expressed by multiplication of the matrices, which are functions of the horizontal differential operators. The involved operators can be released only for very simple side-boundary geometries (e.g., a rectangular plate with simply supported boundaries) or for horizontal boundaries that extend to infinity.

The most popular approach towards a horizontally infinite and layered system is, however, the transformation method in which the Fourier or Hankel transform is used to suppress the horizontal variables $(x, y$ or $r, \theta)$. The

Address reprint requests to Dr. E. Pan, University of Colorado, Department of Civil Engineering, Campus Box 428, Boulder, CO 80309-0428.

Received 6 December 1996; revised 6 May 1997; accepted 23 May 1997

Appl. Math. Modelling 1997, 21:509–521, August

655 Avenue of the Americas, New York, NY 10010

0307-904X/97/$17.00
PII S0307-904X(97)00053-X

transformed coefficients can be found by solving a linear set of first-order differential equations. The exact solutions of these equations are combinations of exponential terms of the vertical variable z (see, e.g., Pan[12,13]). For very thin layers Taylor's series expansion can be used to approximate the exact solutions.[11,21-24] The advantage of this approximation is that by keeping only the linear term[23] numerical inversion of the Fourier or Hankel transform may be avoided; the disadvantage is that the accuracy depends on the thickness of each thin layer, and the results are usually not accurate enough for being used as the Green's functions in the BEM. One therefore needs to resort to the exact solutions for the transformed coefficients.

For a multilayered medium the unknown transformed coefficients in all layers can be solved by forming a global system directly[25,26] or by the finite-layer approaches such as the flexibility matrix method, the stiffness matrix method, or their combination.[22,27-38] When the layer number is relatively large the global system thus formed will become very large, and, consequently, methods of this kind are inefficient for such multilayered media.[39,40]

The best method towards such a medium is the propagator matrix method, which was originated from the work of Thomson,[41] Haskell,[42] and Gilbert and Backus.[43] In this method the transformed coefficients in different layers are related to each other by the multiplication of layer matrices (or propagator matrices), and thus no global system needs to be formed. What is required is to solve at most a 6×6 linear system of algebraic equations for the pure elastic case. When applying the propagator matrix method to elastodynamics care must be taken when the frequency is high since the elements in the layer matrix are growing exponentially with frequency. Some special approaches have been suggested for avoiding this loss-of-precision problem, such as the delta matrix or compound matrix method[44,45] and the generalized reflection/transmission coefficient method.[46-48]

When solving the corresponding static problem it is suggested that one should directly derive the propagator matrix exactly instead of obtaining it approximately from its dynamic counterpart by setting the frequency close to zero. The reasons for this are: (1) all elements in the propagator matrix for the dynamic case are complex functions, while they are usually real for the static case; (2) the structures of the solution are different for these two cases, and one cannot set the frequency exactly to zero in the dynamics; and (3) for the static case one can directly multiply each layer matrix without resorting to complicated methods such as the delta matrix or the generalized reflection/transmission coefficient method, thus saving computational time. Direct solutions for a layered system in elastostatics were derived by Singh,[49] Jovanovich et al.,[50] and Sato and Matsu'ura[51] for the isotropic medium; and by Singh,[52] and Yue and Wang[53] for the transversely isotropic medium. Therefore by using the propagator matrix method the transformed coefficients can be derived exactly without solving a large global system of linear equations. We now need to invert the transformed coefficients to obtain the Green's functions in the physical domain.

Previously, several methods have been proposed for the numerical integration of the transformed coefficients (i.e., the inverse transform), which include the discrete wave number integration[54-56] (which is similar to the FFT method), the modal-summation technique,[57,58] and various numerical quadrature methods as discussed by Dravinski and Mossessian[59] (i.e., the polynomial, spline, Gauss, and the adaptive Clenshaw-Curtis integrations). It is noted that most of these methods were applied to the elastodynamic case only. For the elastostatic case the least squares method, in which the transformed coefficients are approximated by several exponential-polynomial terms with their coefficients being determined by using the method of least squares, was also suggested. This procedure results in a Lipshitz-Hankel-type integral for which an exact quadration can be found.[50,51,60]

In a series of publications[2,12,13,61] the author introduced the cartesian and cylindrical systems of vector functions into the layered structure modeling with focus on the solutions due to either surface loadings or internal dislocations. These two vector systems are extended from the Fourier and Hankel transforms, but they possess certain advantages over the latter transform methods. For one thing the vector function systems can express any integrable vector function, while the Fourier or Hankel transforms can do so for scalar functions only. Another advantage is that, for elastic problems with relatively higher material symmetry, the propagator matrices in these two vector systems are exactly the same and the problems of axially symmetric and two-dimensional deformations can all be included as special cases of the general solution.[12,13] This approach has been extended and applied by Ding and Shen[62] and Huang[63] to some geophysical problems, and by the author[64,65] to the static and dynamic problems in multilayered rectangular plates with simply supported edges.

In this paper the cylindrical system of vector functions and the propagator matrix method are employed to derive the Green's functions in a multilayered transversely isotropic or isotropic half space. Similar to the loss-of-precision problem in the dynamic case when frequency is high, overflow may occur from matrix multiplication when the layer number is large. In order to avoid such a problem we proposed a method in which the layer matrices can be multiplied directly without any overflow, thus the matrix propagation can still be performed very efficiently. In order to numerically integrate the transformed coefficients an adaptive Gauss quadrature with continued fraction expansions[66-69] was adopted and modified. Our experience with this novel numerical quadrature shows that this method possesses the advantage of giving very accurate results (or the results with given accuracy requirement) while using the least quadrature points[61] and thus is superior to previous numerical quadratures. Numerical examples presented in this paper show clearly the effect of material layering and anisotropy on the displacement and stress fields.

2. Green's functions in the transformed domain

We consider a semi-infinite elastic medium made up of $p-1$ parallel, homogeneous, transversely isotropic (or isotropic) layers lying over a homogeneous, transversely isotropic (or isotropic) half space. The layers are numbered serially with the layer at the top being Layer 1 and the half space being Layer p. We place the cylindrical coordinates at the free surface, and the z-axis is drawn down into the medium. The kth layer is bounded by the interfaces $z=z_{k-1}, z_k$. Evidently we have $z_0=0$ and $z_{p-1}=H$, where H is the depth of the last interface. We now introduce the following cylindrical system of vector functions[12,13]

$$\begin{aligned}
\mathbf{L}(r,\theta;\lambda,m) &= \mathbf{e}_z S(r,\theta;\lambda,m)\\
\mathbf{M}(r,\theta;\lambda,m) &= \left(\mathbf{e}_r\frac{\partial}{\partial r}+\mathbf{e}_\theta\frac{\partial}{r\partial\theta}\right)S(r,\theta;\lambda,m)\\
\mathbf{N}(r,\theta;\lambda,m) &= \left(\mathbf{e}_r\frac{\partial}{r\partial\theta}-\mathbf{e}_\theta\frac{\partial}{\partial r}\right)S(r,\theta;\lambda,m)
\end{aligned} \tag{1}$$

with

$$S(r,\theta;\lambda,m)=\frac{1}{\sqrt{2\pi}}J_m(\lambda r)e^{im\theta} \tag{2}$$

where $J_m(\lambda r)$ is the Bessel function of order m with $m=0$ corresponding to the axially symmetric deformation.

We emphasize again that the cylindrical system of vector functions is an extension of the Hankel transform and can be directly applied to a vector function. Since the above cylindrical system (1) forms an orthogonal and complete space, any integrable vector function can be expressed in terms of it. In particular, for the displacement and traction vectors, we have

$$\begin{aligned}
\mathbf{u}(r,\theta,z) &= \sum_m \int_0^{+\infty} [U_L(z)\mathbf{L}(r,\theta)+U_M(z)\mathbf{M}(r,\theta)\\
&\quad +U_N(z)\mathbf{N}(r,\theta)]\lambda\, d\lambda\\
\mathbf{T}(r,\theta,z) &\equiv \sigma_{rz}\mathbf{e}_r+\sigma_{\theta z}\mathbf{e}_\theta+\sigma_{zz}\mathbf{e}_z\\
&= \sum_m \int_0^{+\infty} [T_L(z)\mathbf{L}(r,\theta)+T_M(z)\mathbf{M}(r,\theta)\\
&\quad +T_N(z)\mathbf{N}(r,\theta)]\lambda\, d\lambda
\end{aligned} \tag{3}$$

Substituting equation (3) into the equations of equilibrium and the constitutive relations we obtained two independent sets of simultaneous linear differential equations for U_L, U_M, T_L, T_M, and U_N, T_N, respectively.[12,13] The homogeneous solutions for these two sets can be easily derived and can be expressed in the following compact forms:

$$\begin{aligned}
[E^I(z)] &= [Z^I(z)][K^I]\\
[E^{II}(z)] &= [Z^{II}(z)][K^{II}]
\end{aligned} \tag{4}$$

where

$$\begin{aligned}
[E^I(z)] &= \{U_L(z), \lambda U_M(z), T_L(z)/\lambda, T_M(z)\}^t\\
[E^{II}(z)] &= \{U_N(z), T_N(z)/\lambda\}^t
\end{aligned} \tag{5}$$

are the expansion coefficients, and

$$\begin{aligned}
[K^I] &= \{c_1,c_2,c_3,c_4\}^t\\
[K^{II}] &= \{c_5,c_6\}^t
\end{aligned} \tag{6}$$

are constants to be determined. The solution matrices $[Z^I(z)]$ and $[Z^{II}(z)]$ in equation (4) can be found in other papers by the author.[12,13]

With the homogeneous solutions (4) we can construct the following propagating relation, which relates the expansion coefficients at the top of layer k to those at the bottom of this layer:

$$\begin{aligned}
[E^I(z_{k-1})] &= [a^I][E^I(z_k)]\\
[E^{II}(z_{k-1})] &= [a^{II}][E^{II}(z_k)]
\end{aligned} \tag{7}$$

where z_{k-1} and z_k are the depths of the top and bottom interfaces of layer k, and the matrices $[a^I]$ and $[a^{II}]$ are called propagator matrices (or layer matrices), with their elements being listed in Pan.[12,13]

We now assume, without loss of generality, that there is a point force located along the z-axis at the depth $z=h$, i.e.,

$$f_j(r,\theta,z)=\frac{\delta(r)\delta(\theta)\delta(z-h)}{r}n_j; \qquad j=r,\theta,z \tag{8}$$

where (n_r, n_θ, n_z) are the direction cosines of the unit force vector in the cylindrical coordinates (r, θ, and z). It can be shown that this point force will cause the following discontinuity for the expansion coefficients of the traction vector:

$$\begin{aligned}
\Delta T_L &\equiv T_L(h+0)-T_L(h-0)=\frac{-n_z}{\sqrt{2\pi}}; \qquad m=0\\
\Delta T_M &\equiv T_M(h+0)-T_M(h-0)=\frac{\mp n_x+in_y}{2\lambda\sqrt{2\pi}};\\
&\qquad m=\pm 1\\
\Delta T_N &\equiv T_N(h+0)-T_N(h-0)=\frac{in_x\pm n_y}{2\lambda\sqrt{2\pi}};\\
&\qquad m=\pm 1
\end{aligned} \tag{9}$$

where $i=\sqrt{-1}$, (n_x, n_y, n_z) are the (x, y, z)-direction cosines of the unit force vector in the space-fixed cartesian coordinates, with x- and y-directions being taken, respectively, along $\theta=0$ and $\theta=\pi/2$ of the cylindrical coordinates.

Using these discontinuities the propagating relation (7) and the zero-traction condition at the surface of the layered half space (i.e., at $z=0$), the column matrices $[K^I]$, and $[K^{II}]$ can be determined. Therefore the expansion coefficients in equation (5) at any depth (e.g., for $z \geqslant h$ in layer k, i.e., $z_{k-1} \leqslant z \leqslant z_k$) can be derived exactly as:

$$\begin{aligned}
&[E^I(z)] \\
&\quad = [a_k^I(z-z_{k-1})][a_{k+1}^I]\cdots\left[a_{p-1}^I\right] \\
&\left[Z_p^I(H)\right][K^I] \\
&[E^{II}(z)] \\
&\quad = [a_k^{II}(z-z_{k-1})][a_{k+1}^{II}]\cdots\left[a_{p-1}^{II}\right] \\
&\quad\times\left[Z_p^{II}(H)\right][K^{II}]
\end{aligned} \tag{10}$$

As mentioned earlier overflow may occur from the multiplication of matrices in equation (10). Take the isotropic case for example: It can be shown that the result of multiplication of the propagator matrix $[a_k^I]$ or $[a_k^{II}]$ from layer k to layer $p-1$ is proportional to $\exp\{\lambda(H-z)\}$ which is exponentially growing, while the column matrix $[K^I]$ or $[K^{II}]$ is proportional to $\exp\{-\lambda(H-h)\}$. To overcome this problem we introduce two new propagator matrices $[b_k^I]$ and $[b_k^{II}]$, which are related to the old ones by[61,70]

$$\begin{aligned}
&[a_k^I(z_k-z_{k-1})] \\
&= [b_k^I(z_k-z_{k-1})]\exp\{\lambda(z_k-z_{k-1})\} \\
&[a_k^{II}(z_k-z_{k-1})] \\
&\quad = [b_k^{II}(z_k-z_{k-1})]\exp\{\lambda(z_k-z_{k-1})\}
\end{aligned} \tag{11}$$

where λ is the variable introduced in the cylindrical system of vector functions (1). Since in the new propagator matrices no element is exponentially growing, there will be no overflow problem for a multilayered half space having any number of layers. The exponentially growing term on the right-hand side of equation (11) is canceled out by $\exp\{-\lambda(H-h)\}$ in $[K^I]$ or $[K^{II}]$. Therefore in terms of these new propagator matrices the solutions for the expansion coefficients (10) can be recast into

$$\begin{aligned}
[E^I(z)] &= \exp\{-\lambda d_{zh}\}[b_k^I(z-z_{k-1})] \\
&\quad\times[b_{k+1}^I]\cdots\left[b_{p-1}^I\right][E^I(H)] \\
[E^{II}(z)] &= \exp\{-\lambda d_{zh}\}[b_k^{II}(z-z_{k-1})] \\
&\quad\times[b_{k+1}^{II}]\cdots\left[b_{p-1}^{II}\right][E^{II}(H)]
\end{aligned} \tag{12}$$

where $[E^I(H)]$ and $[E^{II}(H)]$ are known column matrices of the expansion coefficients at $z=H$, and d_{zh} is a constant related to the vertical distance between the field point level z and the source point level h. It is noted that equation (12) is applicable to the case when the field point is below or at the source level, i.e., $z \geqslant h$ and that the matrices $[b^I]$ and $[b^{II}]$ propagate from the homogeneous half space ($z=H$) *upwards*. For the case when the field point is above the source level, similar expressions can be derived in which the matrices $[b^I]$ and $[b^{II}]$ will propagate from the surface ($z=0$) *downwards*. Once the expansion coefficients are determined they can be substituted into equation (3) to get the displacement and traction vectors. The remaining stress components can be calculated using expressions similar to equation (3).[12,13]

3. Green's functions in the physical domain

The Green's functions obtained above in the transformed domain need to be integrated numerically to find the physical domain solutions. Since we have expressed the solutions in terms of the cylindrical system of vector functions the individual components of the Green's functions will be in the cylindrical coordinates. We found that, of the total 27 Green's components, only 15 integrals need to be evaluated.

It is noted that the integrands in the infinite integrals for the Green's functions involve the Bessel function, which is oscillatory and goes to zero slowly when its variable approaches infinity. Thus the common numerical integral methods, such as the trapezoidal rule or Simpson's rule,[71] are not suitable for the current integration. Although the Gauss quadrature has the advantage of giving high accuracy while using few integral points it usually requires recomputation of all the integrands when the order is changed.[72]

In this paper an adaptive Gauss quadrature, developed by Patterson[66,67] and implemented by Chave[69] into a FORTRAN program for the numerical integration of the Hankel transform, is adopted and modified for the evaluation of the Green's functions in multilayered half spaces.

We first express the infinite integral for each Green's function as a summation of partial integration terms:

$$\int_0^{+\infty} f(\lambda, z)J_m(\lambda r)\,d\lambda = \sum_{n=1}^{N}\int_{\lambda_n}^{\lambda_{n+1}} f(\lambda, z)J_m(\lambda r)\,d\lambda \tag{13}$$

In each subinterval a three-point Gauss rule is applied to approximate the integral. A combined relative-absolute error criterion is used to check the results. If the error criterion is not satisfied, new Gauss points are added optimally so that only the new integrand values need to be calculated. This procedure continues until the selected error criterion is satisfied.

It is well known that direct summation is feasible only for rapidly convergent integrals. In order to accelerate the convergence for a slowly convergent series a continued fraction expansion approach is also employed.[68] It was verified[69] that although the continued fraction algorithm is only slightly effective for rapidly convergent series, for slowly convergent ones, the summation behavior is quite dramatic.

The original FORTRAN program was written for one Hankel transform each time. In our case evaluation of 15 infinite integrals is required in order to obtain the total Green's displacements and stresses. Thus direct application of the original adaptive Gauss quadrature would result in a lot of computational time because of the multiplication of the propagator matrices involved. However we noticed that the integrand $f(\lambda, z)$ in equation (13), which represents one of the expansion coefficients in equation (12), is actually the result of the multiplication of the propagator matrices. Since for a given layered half space the propagator matrix depends only upon the integral variable λ the original program can therefore be modified in such a way that for all the Green's components the multiplication of the propagator matrices needs to be evaluated only once for a given Gauss quadrature point λ. It is apparent that such a modification to the original adaptive Gauss quadrature saves a lot of computational time when calculating all the Green's displacements and stresses.

4. Numerical results

Several numerical examples were selected to verify the formulation presented above and to show the effect of material layering and anisotropy on the deformation and stress fields. Results are presented in nondimensional forms and are discussed below.

4.1 Comparison with exact closed-form solutions

The Green's functions in a layered half space can be verified by letting each layer have identical elastic constants and by comparing the results with those from Mindlin's solutions[73] for the isotropic case and Pan and Chou's solutions[74] for the transversely isotropic case.

We assumed a half space composed of three layers with identical elastic properties (i.e., Model 1 in *Table 1*). The interfaces of the layers are at $z = 1.5$ and 2.5 (*Figure 1*).

Table 1. Elastic properties for three models in a three-layered half space

	Model 1		Model 2		Model 3	
	E	ν	E	ν	E	ν
Layer 1	1.0	0.3	1.0	0.3	1.0	0.3
Layer 2	1.0	0.3	2.0	0.3	5.0	0.3
Layer 3	1.0	0.3	4.0	0.3	25.0	0.3

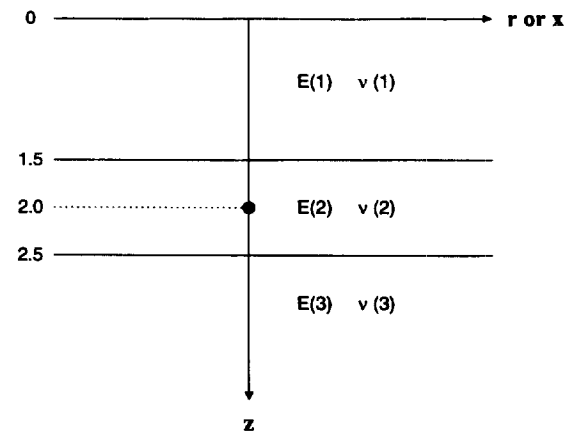

Figure 1. Geometry of a three-layered half-space.

While the point source is located at (0, 0, 2), the field point can be anywhere in the half space. For both isotropic and transversely isotropic cases it was found that the Green's displacements and stresses obtained by the present numerical method agreed with the exact closed-form solutions up to at least seven significant digits, an excellent comparison that could seldom be achieved with previous numerical methods.

4.2 Comparison of results for a half space having different number of layers

We have also argued that our method can be used for multilayered half spaces composed of any number of layers. As a test we divided a homogeneous half space randomly into 50 layers with interfaces at $z = 0.05$, 0.1, 0.15, 0.2, 0.25, 0.3, 0.35, 0.4, 0.45, 0.5, 0.55, 0.6, 0.65, 0.7, 0.75, 0.8, 0.85, 0.9, 0.95, 1.0, 1.1, 1.2, 1.3, 1.4, 1.5, 1.55, 1.6, 1.65, 1.7, 1.75, 1.8, 1.85, 1.9, 1.95, 2.0, 2.05, 2.1, 2.15, 2.2, 2.25, 2.3, 2.4, 2.5, 2.6, 2.7, 2.8, 2.85, 2.9, 3.0. It was found that the Green's functions in this 50-layered half space were exactly the same as those in the 3-layered system (*Figure 1*), which are almost identical to the exact solutions. This comparison indicates that the current method is stable with respect to the layer number. This is another advantage of the present method over some previous ones by which a homogeneous system with different layer number predicts different results.[75]

4.3 Effect of material layering

Having verified our formulation we now study the effect of material layering on the Green's displacements and stresses. We take the three-layered isotropic half space of *Figure 1* as an example. Three models are chosen for this purpose with their elastic properties being given in *Table 1*. While Model 1 actually represents a homogeneous half space, Models 2 and 3 are true layered half spaces having piecewise increasing rigidity with depth. In the following presentation the superscript attached to the Green's displacements or stresses indicates the direction of the point force.

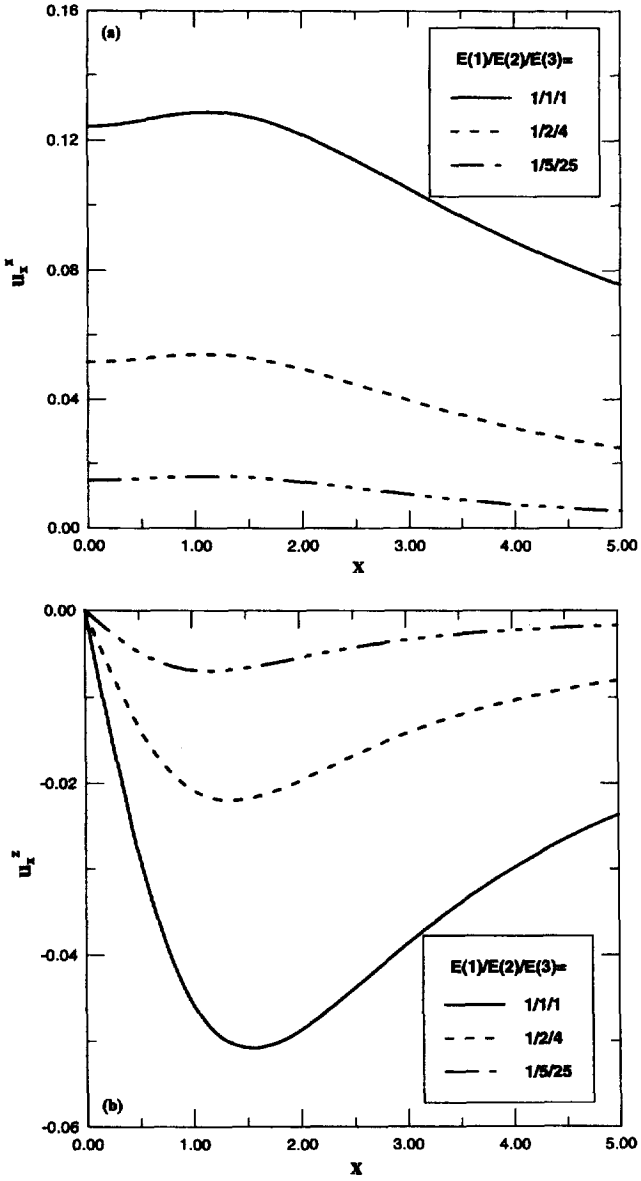

Figure 2. Variation of horizontal displacement components u_x^x in (a) and u_x^z in (b) along the x-axis on the free surface $(0 \rightarrow 5, 0, 0)$. The point force is located at $(0, 0, 2)$ in the three-layered half space of *Figure 1*.

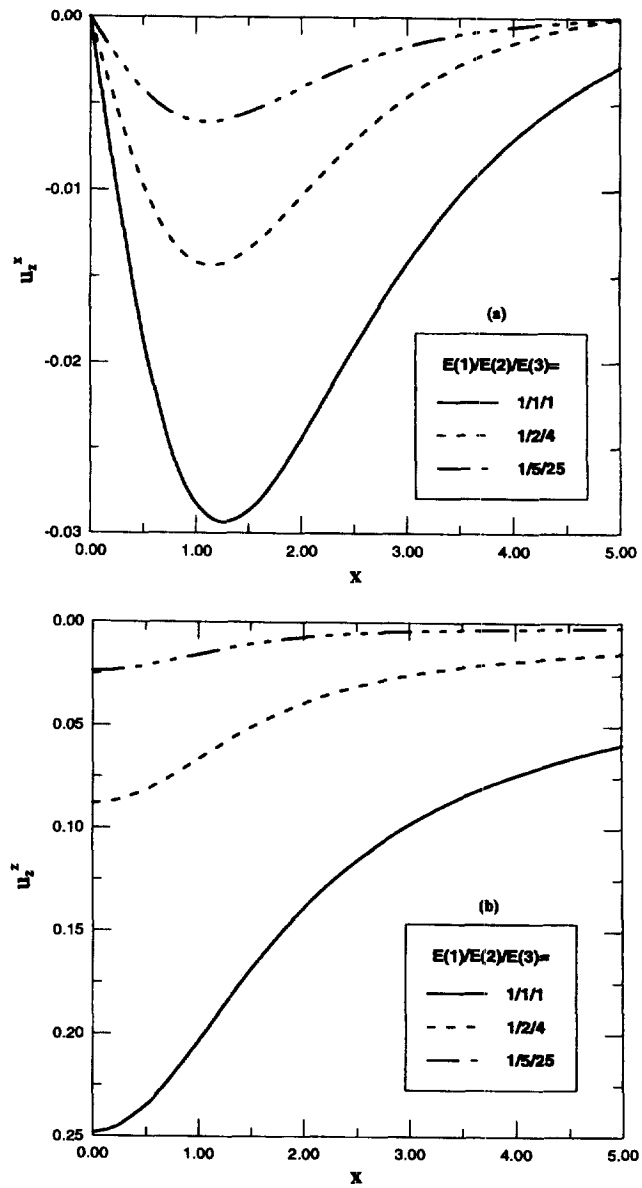

Figure 3. Variation of vertical displacement components u_z^x in (a) and u_z^z in (b) along the x-axis on the free surface $(0 \rightarrow 5, 0, 0)$. The point force is located at $(0, 0, 2)$ in the three-layered half space of *Figure 1*.

Figures 2(a) and *2(b)* show, respectively, variation of the horizontal displacements u_x^x and u_x^z along the x-axis on the free surface $(0 \rightarrow 5, 0, 0)$. The point source is located at $(0, 0, 2)$. As is shown clearly in these figures, increasing Young's modulus decreases the deformability of the layered system. This observation also applies to the vertical displacements u_z^x and u_z^z shown in *Figures 3(a)* and *3(b)*, respectively, where the point source is also located at $(0, 0, 2)$.

It is well known that there is a singularity when the field point is coincident with the source point. The behavior of this singularity can also be affected by the material layering. *Figures 4(a)*, *4(b)*, and *4(c)* show, respectively, variation of the displacement components u_x^x, u_z^x, and u_z^z along the vertical line $(0.05, 0, 0 \rightarrow 5)$. The point source is again located at $(0, 0, 2)$. These figures show similar patterns when the Young's modulus varies; their amplitudes, however, are greatly affected by the increasing rigidity of the layered system and are dominated by the material properties in the source layer. To give a quantitative description of this behavior *Tables 2* and *3* list, respectively, the values of u_x^x and u_z^z. In these two tables the field and source points are on the same vertical line, i.e., the source point is located at $(0, 0, 2)$ while the field point varies as $(0, 0, 1.5 \rightarrow 2.5)$. Both tables indicate that when the field point is close to the source point the displace-

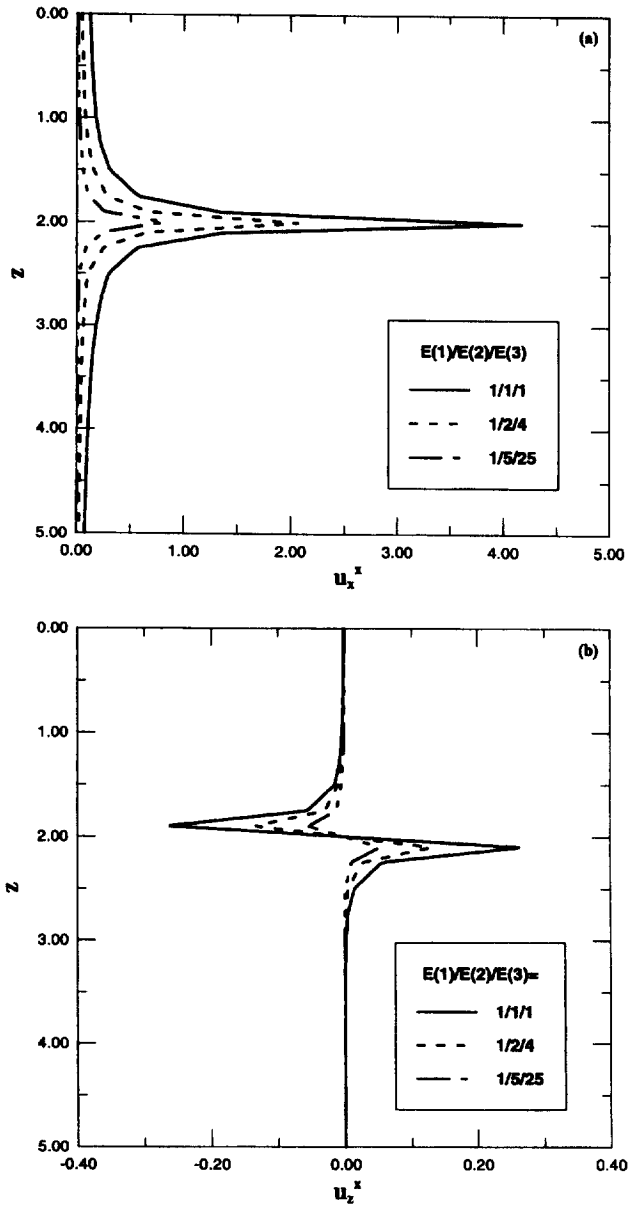

Figure 4. Variation of displacement components u_x^x in (a), u_z^x in (b), and u_z^z in (c) along the vertical line $(0.05, 0, 0 \rightarrow 5)$. The point force is located at (0, 0, 2) in the three-layered half space of *Figure 1*.

ment amplitude increases dramatically and its value is roughly inversely proportional to the Young's modulus in the source layer. For instance at $(0, 0, 1.995)$ we have $u_x^x = 26.64$ for Model 1. Dividing this value, respectively, by the Young's modulus of Models 2 and 3 in the source layer (i.e., $E = 2$ and 5) we get $u_x^x = 13.32$ and 5.33, which are very close to the results listed in *Table 2* for Models 2 and 3, respectively. Furthermore a comparison of *Table 2* with *Table 3* indicates that the vertical displacement has larger amplitude than that of the horizontal one. This is caused by the zero-traction condition on the flat surface $z = 0$.

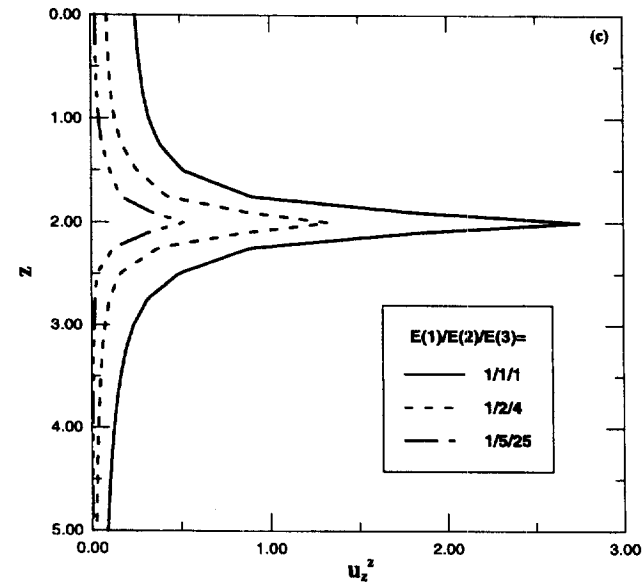

Figure 4. Continued.

Although the Green's displacements close to the singular (source) point for different models are quite different the Green's stresses in the vicinity of the singular point are almost unaffected by the material layering. *Tables 4* and *5* list, respectively, values of stresses σ_{xx}^z and σ_{zz}^z around such a point. It is observed from these tables that close to the singular point (i.e., $(0, 0, 1.995)$ or $(0, 0, 2.005)$) the stress values are nearly the same for different models. Again a comparison of *Table 4* with *Table 5* for the values close to the singular point indicates that the normal stress component in the z-direction has greater amplitude than that in the x-direction, which is again caused by the zero-traction condition on the flat surface $z = 0$.

We have also studied the effect of layering on the stress components when the field and source points are relatively far away from each other. *Figures 5(a)* and *5(b)* show, respectively, the variation of the stresses σ_{xx}^z and σ_{zz}^z along the vertical line $(1, 0, 0 \rightarrow 5)$. The point force is again located at $(0, 0, 2)$. As can be observed from these figures the material layering has a significant influence on the stresses. This is shown clearly in *Figure 5(a)* for the horizontal stress distribution where a material property jump causes discontinuous stress at the interface, with its discontinuity amount proportional to the difference of the Young's moduli in the adjoined layers of the interface.

4.4 *Effect of material anisotropy*

As we mentioned earlier our formulation and program can also be used for multilayered transversely isotropic half spaces. As an example we choose a homogeneous, transversely isotropic half space but artificially divide it into a three-layered system as shown in *Figure 1*. The material properties in each layer are identical with the values $E = 1.0$, $E' = 10.0$, $\nu = \nu' = 0.3$, and $G' = 1.0$, where E and E' are Young's moduli in the plane of transverse

Table 2. Values of u_x^x for the three different layered models

z_f	Model 1 1/1/1	Model 2 1/2/4	Model 3 1/5/25
1.500	0.3092922D+00	0.1567211D+00	0.5931307D − 01
1.750	0.5725805D+00	0.2785454D+00	0.1058214D+00
1.900	0.1369105D+01	0.6696070D+00	0.2597709D+00
1.995	0.2663971D+02	0.1330040D+02	0.5310457D+01
2.005	0.2663962D+02	0.1329988D+02	0.5310072D+01
2.100	0.1367202D+01	0.6590794D+00	0.2520319D+00
2.250	0.5678187D+00	0.2517105D+00	0.8607987D − 01
2.500	0.2997415D+00	0.1048024D+00	0.2153797D − 01

The source is located at (0, 0, 2) and the field point varies as (0, 0, 1.5 → 2.5).

Table 3. Values of u_z^z for the three different layered models

z_f	Model 1 1/1/1	Model 2 1/2/4	Model 3 1/5/25
1.500	0.5172449D+00	0.2588582D+00	0.1056065D+00
1.750	0.9244662D+00	0.4423150D+00	0.1706281D+00
1.900	0.2162221D+01	0.1047322D+01	0.4068943D+00
1.995	0.4147129D+02	0.2069340D+02	0.8261901D+01
2.005	0.4147106D+02	0.2069240D+02	0.8261147D+01
2.100	0.2157676D+01	0.1027284D+01	0.3917459D+00
2.250	0.9130880D+00	0.3913187D+00	0.1319671D+00
2.500	0.4943902D+00	0.1616025D+00	0.3178332D − 01

The source is located at (0, 0, 2) and the field point varies as (0, 0, 1.5 → 2.5).

Table 4. Values of σ_{xx}^z for the three different layered models

z_f	Model 1 1/1/1	Model 2 1/2/4	Model 3 1/5/25
1.500	−0.9929405D − 01	−0.4207813D+00	−0.7784081D+00
1.750	−0.3700344D+00	−0.4275166D+00	−0.4757160D+00
1.900	−0.2278941D+01	−0.2310295D+01	−0.2330077D+01
1.995	−0.9094616D+03	−0.9094895D+03	−0.9095055D+03
2.005	0.9094521D+03	0.9094242D+03	0.9094082D+03
2.100	0.2269355D+01	0.2237154D+01	0.2217291D+01
2.250	0.3601049D+00	0.3021920D+00	0.2591364D+00
2.500	0.8806802D − 01	−0.2012315D+00	−0.4450335D+00

The source is located at (0, 0, 2) and the field point varies as (0, 0, 1.5 → 2.5).

Table 5. Values of σ_{zz}^z for the three different layered models

z_f	Model 1 1/1/1	Model 2 1/2/4	Model 3 1/5/25
1.500	0.7404441D+00	0.5025475D+00	0.2595299D+00
1.750	0.3063320D+01	0.2838989D+01	0.2611179D+01
1.900	0.1929913D+02	0.1910030D+02	0.1890487D+02
1.995	0.7730357D+04	0.7730164D+04	0.7729977D+04
2.005	−0.7730408D+04	−0.7730602D+04	−0.7730789D+04
2.100	−0.1935036D+02	−0.1954814D+02	−0.1973691D+02
2.250	−0.3114926D+01	−0.3335968D+01	−0.3545096D+01
2.500	−0.7933940D+00	−0.1034185D+01	−0.1269552D+01

The source is located at (0, 0, 2) and the field point varies as (0, 0, 1.5 → 2.5).

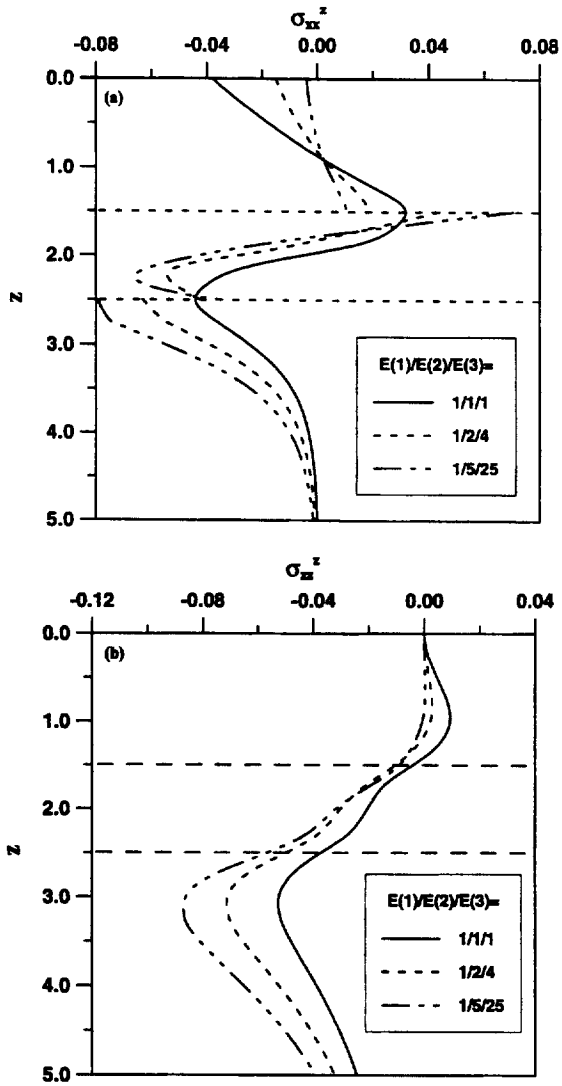

Figure 5. Variation of stress components σ_{xx}^z in (a) and σ_{zz}^z in (b) along the vertical line $(1,0,0 \rightarrow 5)$. The point force is located at $(0,0,2)$ in the three-layered half space of *Figure 1*.

isotropy and in a direction normal to it, respectively, ν and ν' are Poisson's ratios, characterizing the lateral strain response in the plane of transverse isotropy to a stress acting parallel and normal to it, and G' is the shear modulus in planes normal to the plane of transverse isotropy.

For the source point located at $(0,0,2)$ we calculated the displacement and stress distributions at the free surface and compared the results with those from the isotropic model (i.e., Model 1 in *Table 1*). For the convenience of presentation the transversely isotropic and isotropic cases are denoted, respectively, by the TI-case and the I-case.

Figures 6(a) and *6(b)* show, respectively, the surface deflection contours of u_z^z for the I- and TI-cases caused by a vertical point force. As can be easily observed these contours have similar patterns (the deformation is axially symmetric with a maximum deflection at the center that is at the same vertical line with the source point) but the TI-case predicts a much smaller amplitude than the I-case (e.g., at the center we have $u_z^z = 0.24828$ for the I-case and 0.10037 for the TI-case).

Figures 7(a) and *7(b)* show, respectively, the surface deflection contours of u_z^x for the I- and TI-cases caused by a horizontal point force. For this displacement component the deformation is antisymmetric with respect to the y-axis and symmetric with respect to the x-axis. Compared to the I-case the TI-case predicts not only smaller amplitude of the surface deflection, but also a different contour pattern (e.g., the maximum amplitude for this displacement is $u_z^x = 0.029$ at $(x, y) = (-1.5, 0)$ for the I-case and 0.009 at $(x, y) = (-0.5, 0)$ for the TI-case).

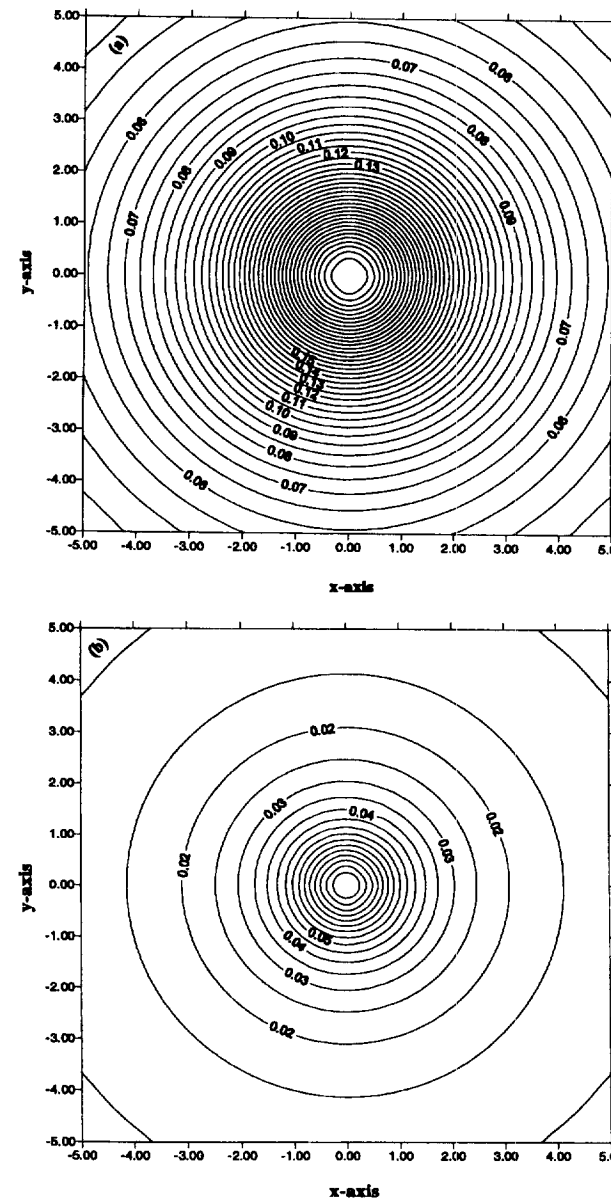

Figure 6. Displacement contours of u_z^z at the free surface caused by a vertical point force at $(0,0,2)$ in the three-layered half space of *Figure 1*. (a) is the isotropic case, and (b) is the transversely isotropic case.

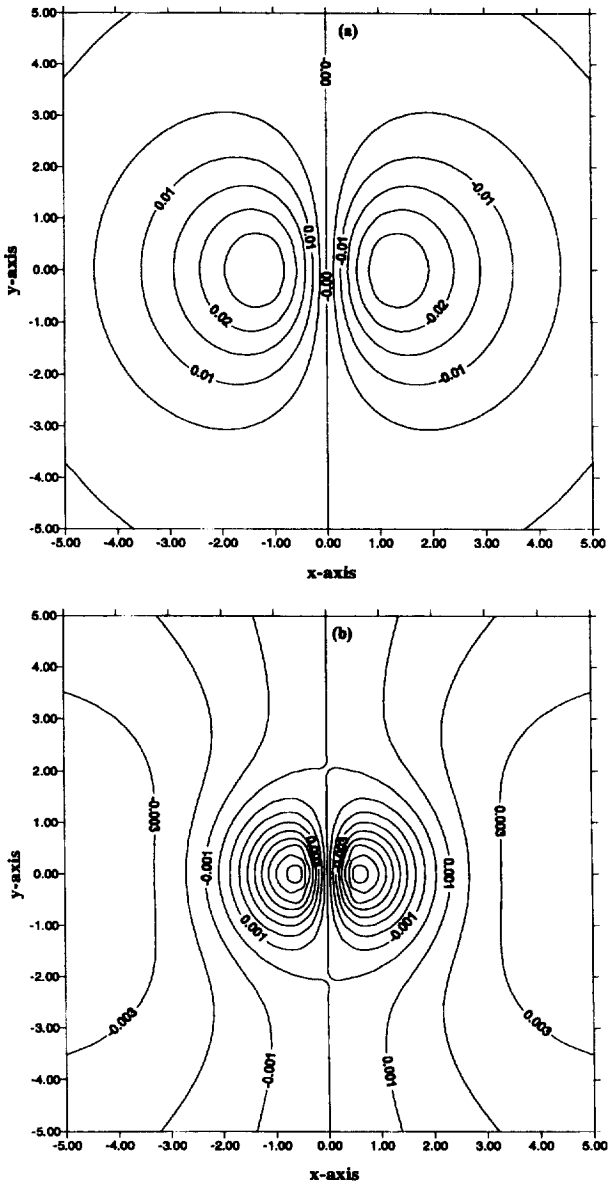

Figure 7. Displacement contours of u_z^x at the free surface caused by a horizontal point force at (0, 0, 2) in the three-layered half space of *Figure 1*. (a) is the isotropic case, and (b) is the transversely isotropic case.

A third contour comparison is for the surface horizontal displacement u_x^x as shown in *Figures 8(a)* and *8(b)*, respectively, for the I- and TI-cases. The deformation is symmetric with respect to both the x- and y-axes. We noticed that for this component the maximum amplitudes for the I- and TI-cases are very close ($u_x^x = 0.128$ at $(x, y) = (1.0, 0)$ for the I-case and 0.136 at $(x, y) = (0.5, 0)$ for the TI-case). This is due to the fact that in the horizontal direction both the I- and TI-cases have the same Young's modulus $E = 1$.

We have also compared the stress contours. While *Figures 9(a)* and *9(b)* show, respectively, the stress contours of σ_{xx}^x for the I- and TI-cases caused by a point force in the horizontal direction, *Figures 10(a)* and *10(b)* show, respectively, the stress contours of σ_{xx}^z for the I- and TI-cases caused by a point force in the vertical direction. On observation of these figures we noticed that all these contours have the x- or y-axis as either their symmetric or antisymmetric axis, but the stress patterns and magnitudes are different because of the effect of anisotropy. For instance for σ_{xx}^x along the positive x-axis there is a maximum (0.010 at $x = 0.5$) and a minimum (-0.015 at $x = 3.0$) for the I-case (*Figure 9[a]*), but only a minimum (-0.026 at $x = 1.5$) for the TI-case (*Figure 9[b]*). For the stress contours of σ_{xx}^z (*Figures 10[a]* and *10[b]*) we noticed that, although their patterns are similar, the non-zero domain is concentrated in a smaller region

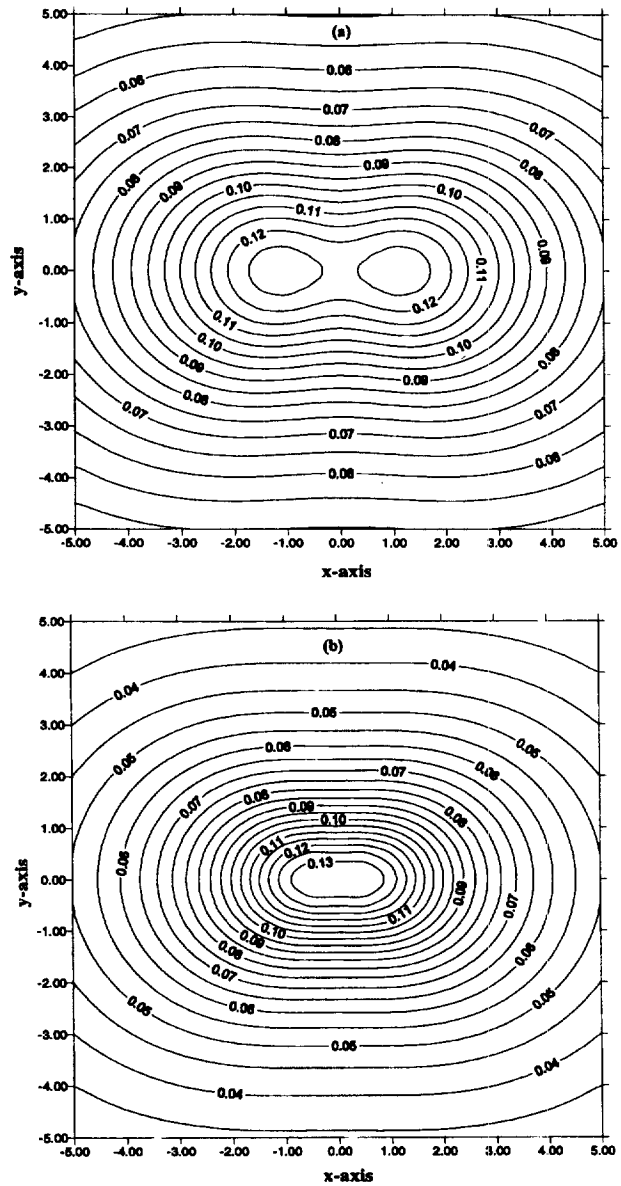

Figure 8. Displacement contours of u_x^x at the free surface caused by a horizontal point force at (0, 0, 2) in the three-layered half space of *Figure 1*. (a) is the isotropic case, and (b) is the transversely isotropic case.

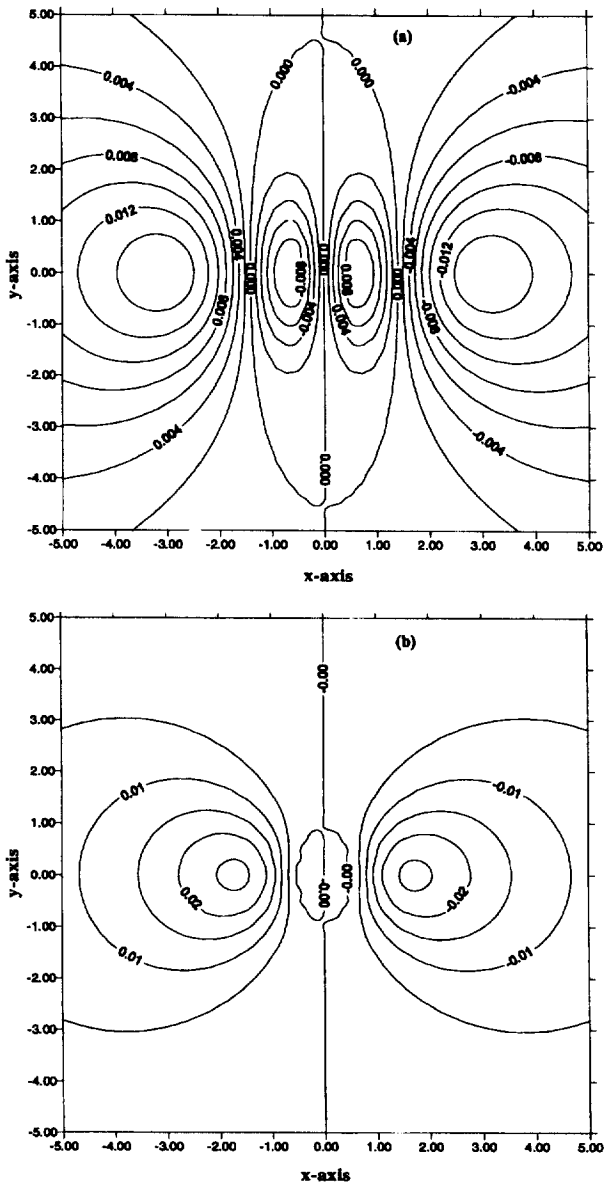

Figure 9. Stress contours of σ_{xx}^{x} at the free surface caused by a horizontal point force at (0, 0, 2) in the three-layered half space of *Figure 1*. (a) is the isotropic case, and (b) is the transversely isotropic case.

for the TI-case than for the I-case. This is again a clear effect of material anisotropy.

5. Conclusions

In this paper we derived the formulation for the calculation of the three-dimensional Green's functions in multilayered transversely isotropic or isotropic half spaces. The formulation is based on the cylindrical system of vector functions combined with the propagator matrix method. The Green's solutions are expressed in terms of infinite integrals involving Bessel functions and are numerically integrated by an adaptive Gauss quadrature with continuous fraction expansions. Numerical examples presented in this paper show that the proposed method is both accurate and efficient; at the same time, the effect of material layering and anisotropy has been clearly shown through these examples. While the numerical results may have applications in different areas where layered structures are involved the Green's functions developed in this paper will be implemented to the author's three-dimensional BEM code[76] to study problems involving complicated geometry and loading conditions in layered systems.

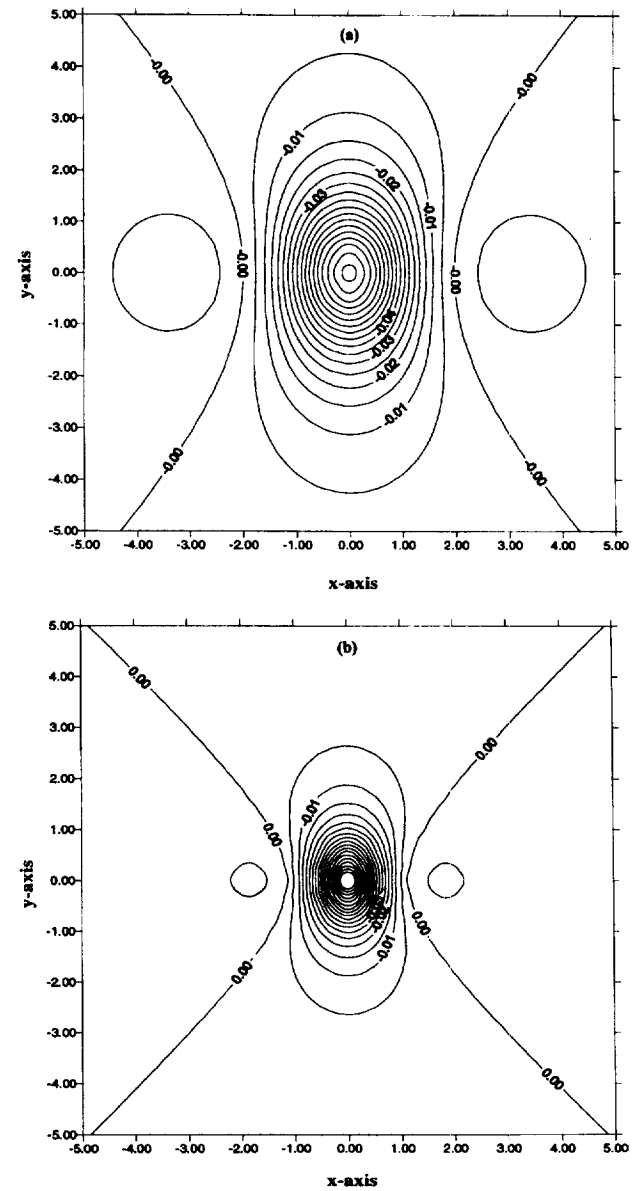

Figure 10. Stress contours of σ_{xx}^{z} at the free surface caused by a vertical point force at (0, 0, 2) in the three-layered half space of *Figure 1*. (a) is the isotropic case, and (b) is the transversely isotropic case.

Acknowledgment

Part of this work was conducted in 1995 while the author was affiliated with the Department of Mechanical Engineering. He would like to thank Profs. T. L. Geers and M. L. Dunn for their constructive comments on this paper. Support from National Science Foundation under Grant CMS-9622645 is greatly appreciated.

References

1. Crampin, S. A review of wave motion in anisotropic and cracked elastic-media. *Wave Motion* 1981, **3**, 343–391
2. Pan, E. Thermoelastic deformation of a transversely isotropic and layered half-space by surface loads and internal sources. *Phys. Earth Planet. Inter.* 1990, **60**, 254–264
3. Yin, W. L. Thermal stresses in anisotropic multilayered structures. *Thermal Stress and Strain in Microelectronics Packaging*, ed. J. Lau, Van Nostrand-Reinhold, New York, 1993, pp. 95–138
4. Zouari, K, and Lee, Y. C. Stress analysis of the vertical interconnect for three-dimensional packaging. *J. Electronic Packaging* 1991, **113**, 233–239
5. Daniel, I. M., Wang, T. M. and Gotro, J. T. Thermomechanical behavior of multilayer structures in microelectronics. *J. Electronic Packaging* 1990, **112**, 11–15
6. Wait, J. R. *Electromagnetic Waves in Stratified Media*. Pergamon Press, New York, 1970
7. Selvadurai, A. P. S. and Yue, Z. Q. On the indentation of a poroelastic layer. *Int. J. Numer. Anal. Methods Geomech.* 1994, **18**, 161–175
8. Senjuntichai, T. and Rajapakse, R. K. N. D. Exact stiffness method for quasi-statics of a multi-layered poroelastic medium. *Int. J. Solids Struct.* 1995, **32**, 1535–1553
9. Cathles, L. M. *The Viscosity of the Earth's Mantle*. Princeton University Press, Princeton, NJ, 1975
10. Booker, J. R. and Small, J. C. Finite layer analysis of viscoelastic layered materials. *Int. J. Numer. Anal. Methods Geomech.* 1986, **10**, 415–430
11. Seale, S. H. and Kausel, E. Point loads in cross-anisotropic, layered halfspaces. *J. Eng. Mech.* 1989, **115**, 509–524
12. Pan, E. Static response of a transversely isotropic and layered half-space to general surface loads. *Phys. Earth Planet. Inter.* 1989, **54**, 353–363
13. Pan, E. Static resporse of a transversely isotropic and layered half-space to general dislocation sources. *Phys. Earth Planet. Inter.* 1989, **58**, 103–117
14. Kennett, B. L. N. Elastic wave propagation in stratified media. *Advances in Applied Mechanics*, Volume **21**, ed. C. S. Yih, Academic Press, New York, 1981, pp. 79–167
15. Kennett, B. L. N. *Seismic Wave Propagation in Stratified Media*, Cambridge University Press, New York, 1983
16. Ju, T. H. Analysis of fracture in composite laminated plates. Ph.D. Thesis, University of Colorado at Boulder, 1991
17. Bahar, L. Y. A state space approach to elasticity. *J. Franklin Institute* 1975, **299**, 33–41
18. Rao, N. S. V. K. and Das, Y. C. A mixed method in elasticity. *J. Appl. Mech.* 1977, **44**, 51–56
19. Abhyankar, N. S. and Chandrashekara, S. Concise expressions for the dispersion relations for waves in an infinite isotropic plate. *Mech. Res. Commun.* 1990, **17**, 409–414
20. Chandrashekara, S. and Santhosh, U. An efficient solution to the free vibration of thick angle-ply laminae. *Int. J. Solids Struct.* 1991, **27**, 999–1010
21. Waas, G. Linear two-dimensional analysis of soil dynamics problems in semi-infinite layer media. Ph.D. Thesis, University of California, Berkeley, 1972
22. Kausel, E. and Roesset, J. M. Stiffness matrices for layered soils. *Bull. Seism. Soc. Am.* 1981, **71**, 1743–1761
23. Kausel, E. and Seale, S. H. Static loads in layered halfspaces. *J. Appl. Mech.* 1987, **54**, 403–408
24. Datta, S. K., Shah, A. H. and Karunasena, W. Wave propagation in composite media and material characterization. *Elastic Waves and Ultrasonic Nondestructive Evaluation*, ed. S. K. Datta, J. D. Achenbach and Y. S. Rajapaske, Elsevier Science Publishers B. V., North-Holland, 1990, pp. 159–169
25. Mal, A. K. Guided waves in layered solids with interface zones. *Int. J. Eng. Sci.* 1988, **26**, 873–881
26. Mal, A. K. Wave propagation in layered composite laminates under periodic surface loads. *Wave Motion* 1988, **10**, 257–266
27. Biot, M. A. A new approach to the mechanics of orthotropic multilayered plates. *Int. J. Solids Struct.* 1972, **8**, 475–490
28. Biot, M. A. Simplified dynamics of multilayered orthotropic viscoelastic plates. *Int. J. Solids Struct.* 1972, **8**, 491–509
29. Biot, M. A. Buckling and dynamics of multilayered and laminated plates under initial stress. *Int. J. Solids Struct.* 1974, **10**, 419–451
30. Biot, M. A. Fundamentals of generalized rigidity matrices for multi-layered media. *Bull. Seismol. Soc. Am.* 1983, **73**, 749–763
31. Small, J. C. and Booker, J. R. Finite layer analysis of layered elastic materials using a flexibility approach. Part 1—Strip loadings. *Int. J. Numer. Methods Eng.* 1984, **20**, 1025–1037
32. Small, J. C. and Booker, J. R. Finite layer analysis of layered elastic materials using a flexibility approach. Part 2—Circular and rectangular loadings. *Int. J. Numer. Methods Eng.* 1986, **23**, 959–978
33. Choi, H. J. and Thangjitham, S. Stress analysis of multilayered anisotropic elastic media. *J. Appl. Mech.* 1991, **58**, 382–387
34. Thangjitham, S. and Choi, H. J. Thermal stresses in a multilayered anisotropic medium. *J. Appl. Mech.* 1991, **58**, 1021–1027
35. Pindera, M. J. and Lane, M. S. Frictionless contact of layered half-planes. Part I: Analysis. *J. Appl. Mech.* 1993, **60**, 633–639
36. Pindera, M. J. and Lane, M. S. Frictionless contact of layered half-planes. Part II: Numerical results. *J. Appl. Mech.* 1993, **60**, 640–645
37. Wang, Y. and Rajapakse, R. K. N. D. An exact stiffness method for elastodynamics of a layered orthotropic half-plane. *J. Appl. Mech.* 1994, **61**, 339–348
38. Kuo, C. H. and Keer, L. M. Three-dimensional analysis of cracking in a multilayered composite. *J. Appl. Mech.* 1995, **62**, 273–278
39. Lin, W. and Keer, L. M. Analysis of a vertical crack in a multilayered medium. *J. Appl. Mech.* 1989, **56**, 63–69
40. Lin, W. and Keer, L. M. Three-dimensional analysis of cracks in layered transversely isotropic media. *Proc. R. Soc. Lond. A* 1989, **424**, 307–322
41. Thomson, W. T. Transmission of elastic waves through a stratified medium. *J. Appl. Phys.* 1950, **21**, 89–93
42. Haskell, A. The dispersion of surface waves on a multilayered media. *Bull. Seism. Soc. Am.* 1953, **43**, 17–34
43. Gilbert, F. and Backus, G. Propagator matrices in elastic wave and vibration problems. *Geophys.* 1966, **31**, 326–332
44. Dunkin, J. W. Computation of modal solutions in layered elastic media at high frequencies. *Bull. Seism. Soc. Am.* 1965, **55**, 335–358
45. Schwab, F. and Knopoff, L. Surface wave dispersion computations. *Bull. Seism. Soc. Am.* 1970, **60**, 321–344
46. Apsel, R. J. Dynamic Green's functions for layered media and applications to boundary value problem. Ph.D. Thesis, University of California at San Diego, 1979
47. Luco, J. E. and Apsel, R. J. On the Green's function for a layered half-space, Part I. *Bull. Seism. Soc. Am.* 1983, **73**, 909–929
48. Chen, X. A systematic and efficient method of computing normal modes for multilayered half-space. *Geophys. J. Int.* 1993, **115**, 391–409
49. Singh, S. J. Static deformation of a multilayered half-space by internal sources. *J. Geophys. Res.* 1970, **75**, 3257–3263
50. Jovanovich, D. B., Husseini, M. I. and Chinnery, M. A. Elastic dislocations in a layered half-space—I. Basic theory and numerical methods. *Geophys. J. R. Astro. Soc.* 1974, **39**, 205–217
51. Sato, R. ånd Matsu'ura, M. Static deformations due to the fault spreading over several layers in a multi-layered medium, Part I: Displacement. *J. Phys. Earth* 1973, **21**, 227–249
52. Singh, S. J. Static deformation of a transversely isotropic multilayered half-space by surface loads. *Phys. Earth Planet. Inter.* 1986, **42**, 263–273

53. Yue, Z. Q. and Wang, R. Static solution for transversely isotropic elastic n-layered systems. *Acta Scientiarum Naturalium*, Universitatis Pekinensis 1988, **24**, 202–211
54. Bouchon, M. and Aki, K. Discrete wavenumber representation of seismic source wave fields. *Bull. Seism. Soc. Am.* 1977, **67**, 259–277
55. Bouchon, M. Discrete wave number representation of elastic wave fields in three-space dimensions. *J. Geophys. Res.* 1979, **84**, 3609–3614
56. Bouchon, M. A simple method to calculate Green's functions for elastic layered media. *Bull. Seism. Soc. Am.* 1981, **71**, 959–971
57. Zhu, J., Shah, A. H. and Datta, S. K. Modal representation of two-dimensional elastodynamic Green's functions. *J. Eng. Mech.* 1995, **121**, 26–36
58. Zhu, J., Shah, A. H. and Datta, S. K. The evaluation of Cauchy principal value integrals and weakly singular integrals in BEM and their applications. *Int. J. Numer. Meth. Eng.* 1996, **39**, 1017–1028
59. Dravinski, M. and Mossessian, T. K. On evaluation of the Green's functions for harmonic line loads in a viscoelastic half space. *Int. J. Numer. Meth. Eng.* 1988, **26**, 823–841
60. Chan, K. S., Karasudhi, P. and Lee, S. L. Force at a point in the interior of a layered elastic half space. *Int. J. Solids Struct.* 1974, **10**, 1179–1199
61. Pan, E. The static response of multilayered foundations to general surface loading and body force. *Acta Mechanica Sinica* 1989, **21**, 344–353
62. Ding, Z. Y. and Shen, Y. Q. Quasi-static response of a layered viscoelastic half-space to general surface loading. *Phys. Earth Planet. Inter.* 1991, **66**, 278–289
63. Huang, J. The general model of static responses in multilayered elastic media. *Crust. Deform. Earthquake* 1991, **11**, 1–6
64. Pan, E. An exact solution for transversely isotropic, simply supported and layered rectangular plates. *J. Elasticity* 1991, **25**, 101–116
65. Pan, E. Vibration of a transversely isotropic, simply supported and layered rectangular plate. *J. Elasticity* 1992, **27**, 167–181
66. Patterson, T. N. L. The optimum addition of points to quadrature formulae. *Math. Comp.* 1968, **22**, 847–856
67. Patterson, T. N. L. Algorithm for automatic numerical integration over a finite interval [D1]. *Commun. ACM* 1973, **16**, 694–699
68. Hanggi, P., Roesel, F. and Trautmann, P. Evaluation of infinite series by use of continued fraction expansions: A numerical study. *J. Comp. Phys.* 1980, **37**, 252–258
69. Chave, A. D. Numerical integration of related Hankel transforms by quadrature and continued fraction expansion. *Geophys.* 1983, **48**, 1671–1686
70. Sato, R. Crustal deformation due to dislocation in a multi-layered medium. *J. Phys. Earth* 1971, **19**, 31–46
71. Davis, P. J. and Rabinowitz, P. *Methods of Numerical Integration*, Academic Press, New York, 1975
72. Kundu, T. Computation of surface motion in a stratified half space. Ph.D. Thesis, University of California at Los Angeles, 1983
73. Mindlin, R. D. Force at a point in the interior of a semi-infinite solid. *Physics* 1936, **7**, 195–202
74. Pan, Y. C. and Chou, T. W. Green's function solutions for semi-infinite transversely isotropic materials. *Int. J. Eng. Sci.* 1979, **17**, 545–551
75. Wideberg, J. and Benitez, F. G. Elastic stress and displacement distribution in an orthotropic multilayered system due to a concentrated load. *Eng. Anal. Boundary Elements* 1995, **16**, 19–27
76. Pan, E. and Amadei, B. 3-D boundary element formulation of anisotropic elasticity with gravity. *Appl. Math. Modelling* 1996, **20**, 114–120